Investigation of coarse-graining parameters for super-grid LEM closure applied to LES of practical bluff-body flames

Citation for the original published paper (version of record):
Murlidharan Menon, A., Kerstein, A., Oevermann, M. (2024). Investigation of coarse-graining parameters for super-grid LEM closure applied to LES of practical bluff-body flames. Combustion Theory and Modelling, In Press.
http://dx.doi.org/10.1080/13647830.2024.2428156

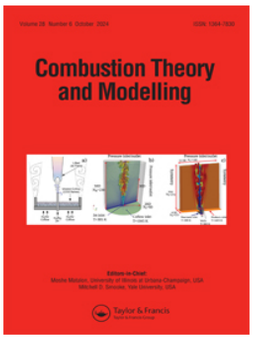

Taylor & Francis
Taylor & Francis Group

Combustion Theory and Modelling

ISSN: (Print) (Online) Journal homepage: www.tandfonline.com/journals/tctm20

Investigation of coarse-graining parameters for super-grid LEM closure applied to LES of practical bluff-body flames

Abhilash M. Menon, Alan Kerstein & Michael Oevermann

To cite this article: Abhilash M. Menon, Alan Kerstein & Michael Oevermann (16 Nov 2024): Investigation of coarse-graining parameters for super-grid LEM closure applied to LES of practical bluff-body flames, Combustion Theory and Modelling, DOI: 10.1080/13647830.2024.2428156

To link to this article: https://doi.org/10.1080/13647830.2024.2428156

Published online: 16 Nov 2024.

Combustion Theory and Modelling, 2024
https://doi.org/10.1080/13647830.2024.2428156

Taylor & Francis
Taylor & Francis Group

Investigation of coarse-graining parameters for super-grid LEM closure applied to LES of practical bluff-body flames

Abhilash M. Menon[a*], Alan Kerstein[b] and Michael Oevermann[a,c]

[a]*Mechanics and Maritime Sciences (M2), Chalmers Tekniska Högskola, Göteborg, Sweden* [b]*Independent Consultant, Danville, CA, USA* [c]*Chair of Numerical Mathematics and Scientific Computing, Brandenburgische Technische Universität Cottbus-Senftenberg (BTU), Cottbus, Germany*

(*Received 16 May 2024; accepted 25 October 2024*)

Large Eddy Simulation (LES) coupled with the Linear Eddy Model (LEM) provides a robust method for studying turbulent combustion, but it is computationally expensive due to the need for highly resolved sub-grid LEM domains. These domains simulate sub-grid stirring through stochastic rearrangements of scalar fields, while large-scale transport is modelled using a Lagrangian 'splicing' scheme. To address the computational cost of LES-LEM, a super-grid (SG) framework for LEM closure was developed by the authors (Comb. Theor. Model. 28, 2024), which uses coarse-graining, on-the-fly chemistry tabulation and a presumed PDF approach to reconstruct thermochemical fields at LES resolution. This study applies SG-LEM to a challenging setup, Case 1 of the Volvo Validation Rig, which involves a bluff-body-stabilised turbulent premixed propane-air flame, as a stress test to identify limitations that were not revealed by the previous application, in particular that of the coarse-graining parameters used to generate the super-grid. The intent is to yield a more realistically constrained assessment of the current capabilities of the method, and insight into possible ways for improving it. Four simulations were conducted using three SG cluster sizes. The finest resolution was tested with a global 2-step mechanism, showing good agreement with experimental data for temperature and velocity, particularly near the bluff body. The two larger cluster sizes used a 66-step skeletal mechanism for more detailed chemical closure but led to unphysical quenching due to splicing inaccuracies. To mitigate these issues, two novel additions were introduced: an intra-cluster-stirring routine and a method to control SG cluster shapes to reduce numerical dissipation. These methods improved flame stability with coarser SG clusters and more detailed mechanisms. Comparison with experiments showed good agreement for temperature and velocity, though elevated CO levels were observed in the recirculation region. Potential methods for further improving SG-LEM's capabilities are discussed.

Keywords: LES-LEM; premixed flames; stabilised flames; turbulence modelling; subgrid-scale closure

1. Introduction

Large Eddy Simulation (LES) is increasingly utilised in turbulent combustion simulation [1], often showing favourable comparisons with RANS-based techniques (Reynolds

*Corresponding author. Email: menona@chalmers.se; menonabhilash89@gmail.com

averaged Navier Stokes). Unlike RANS, which models turbulence, LES directly resolves turbulent structures limited by mesh resolution. This characteristic makes LES more suitable for modelling transient phenomena such as extinction-reignition processes and cycle-to-cycle variations in internal combustion engines (ICEs). Combustion LES involves the evolution of transport equations for filtered continuity, momentum, species concentrations (or mass fractions) and energy. Proper treatment of the unresolved sub-grid scale (SGS) effects of advection, diffusion and chemical source terms is essential, often addressed through various turbulence-chemistry-interaction (TCI) treatments. Chemical closure methods generally fall into two categories: (1) 'mapping' or (2) 'reaction-rate' closure. Reaction-rate closures necessitate the advancement of all species transport equations as well as that of energy, requiring models for the chemical source terms, including species concentrations and sometimes heat release, e.g. sensible enthalpy transport. These steps involve numerical integration of stiff chemical ordinary differential equations (ODEs), demanding significant computational effort compared to mapping-type closure models. Mapping-type closures, on the other hand, aim to decouple chemistry and flow computation by advancing a reduced set of transport equations, often constituting a reduced manifold such as mixture fraction and progress variable. This reduced set is then used to directly map species mass fractions, density, and temperature from a separate, often pre-computed, solution space. Mapping closures often employ a generic representation or structure of the flame front, typically referred to as a 'flamelet', which can incorporate diffusion and flame stretch effects.

This study involves the novel super-grid Linear Eddy Model (SG-LEM), which was introduced by the authors in Ref. [2]. It is based on the Linear Eddy Model (LEM) of Kerstein [3] but used in a novel super-grid (SG) configuration. The SGs are generated by coarse-graining of the LES mesh, and a presumed PDF mapping approach is used to regain scalar fields at LES resolution. Thus, the method could be classified as a hybrid of the aforementioned closure types wherein reduced scalar manifolds are generated *in-situ* and on-the-fly by multiple one-dimensional LEM domains that are time-advanced in parallel to the LES flow solver. The method was validated against DNS data for a recirculation-stabilised, premixed ethylene-air flame where it demonstrated significant computational speed-up – estimated to nearly 20x relative to LES-LEM, and 2x relative to Partially-Stirred Reactor (PaSR) [4] closure. SG-LEM was able to produce more accurate temperature and concentration fields than PaSR, especially for intermediate and radical species CO and OH, respectively. Formulation of the SG-LEM framework will be discussed later in the text, however, it can already be inferred that speed-up and accuracy of the results should depend on coarse-graining parameters such as the cluster size. The DNS case investigated in [2] showed nearly identical concentration fields for tested cluster sizes 125 and 1000. This could be due to the small geometry typical of DNS cases, as well as the high temperature (1125 K) of the fuel-air mixture which allowed for easy ignition; hence, further investigation is needed to establish the response behaviour of the SG-LEM framework to coarse-graining (or clustering) parameters, and limitations that may arise, given that the overall approach is broadly promising as an eventual state-of-the-art technique.

In this follow-up work to Ref. [2], SG-LEM will be used to simulate the Volvo Validation Rig. Compared to the previous application, the setup consists of a larger geometry, and a propane-air fuel mixture at atmospheric conditions. The larger geometry, akin to practical flames, would allow for a more realistic test of the coarse-grained approach that is central to the current SG-LEM framework and which directly affects large-scale transport (or 'splicing') of LEM domain fragments as will be discussed. Additionally, the high

Reynolds Number (*Re*) of the case provides an opportunity to apply SG-LEM in the *Re* regime for which it is most cost-effective relative to alternatives and which is the regime of greatest practical interest. Experimental studies by Sjunnesson et al. [5–7] provide time-averaged and root-mean-square (RMS) measurements for velocity, temperature and CO mass fractions, as well as statistical distributions for selected quantities such as temperature. The Volvo setup has been the subject of several LES studies in the past [see 8–12], which are used as reference for the current study.

The paper is structured as follows: Section 2 presents the governing equations of reactive LES; Section 3 introduces combustion modelling using LEM and SG-LEM; Section 4 describes the test case and numerical implementations; Section 5 analyses the results followed by a discussion.

2. Reactive LES formulation

The Favre filtered LES equations for global mass, momentum, species mass and enthalpy are [13]:

$$\begin{aligned}
\frac{\partial \bar{\rho}}{\partial t} + \frac{\partial \bar{\rho}\tilde{u}_i}{\partial x_i} &= 0, \\
\frac{\partial \bar{\rho}\tilde{u}_i}{\partial t} + \frac{\partial \bar{\rho}\tilde{u}_i\tilde{u}_j}{\partial x_j} &= -\frac{\partial \bar{p}}{\partial x_i} + \frac{\partial}{\partial x_j}\left(\bar{\tau}_{ji} + \bar{\tau}_{ji}^{\mathrm{sgs}}\right), \\
\frac{\partial \bar{\rho}\tilde{Y}_\alpha}{\partial t} + \frac{\partial \bar{\rho}\tilde{u}_j\tilde{Y}_\alpha}{\partial x_j} &= -\frac{\partial}{\partial x_j}\left(\bar{j}_{\alpha,j} + \bar{j}_{\alpha,j}^{\mathrm{sgs}}\right) + \bar{S}_\alpha, \\
\frac{\partial \bar{\rho}\tilde{h}}{\partial t} + \frac{\partial \bar{\rho}\tilde{u}_j\tilde{h}}{\partial x_j} &= \tilde{u}_j\frac{\partial \bar{p}}{\partial x_j} + \frac{\partial}{\partial x_j}\left(D_{\mathrm{eff}}\frac{\partial \tilde{h}}{\partial x_j}\right) + \frac{\partial \bar{p}}{\partial t}.
\end{aligned} \tag{1}$$

Here, t denotes time, x_j is the spatial coordinate, ρ is density, u_i is velocity, p is pressure, Y_α is the mass fraction of specie α, T is temperature, D_{eff} the effective diffusivity and h is the chemical enthalpy. The operators $\tilde{}$ and $\bar{}$ represent Favre-filtering and spatial filtering, respectively. The box filter kernel is used for spatial filtering in this work. Chemical enthalpy is defined as[1]

$$h = \sum Y_\alpha h_\alpha, \tag{2}$$

where species enthalpy h_α relates to the standard formation enthalpy, h_α^0, via the caloric equation of state as

$$h_\alpha(T) = h_\alpha^0 + \int_{T^0}^{T} c_{p,\alpha}(T)\,\mathrm{d}T. \tag{3}$$

Here, $c_{p,\alpha}$ represents the specific heat of specie α at constant pressure. τ_{ij} and $j_{\alpha,j}$ are the stress tensor and species diffusive flux, while their unresolved counterparts are τ_{ij}^{sgs} and $j_{\alpha,j}^{\mathrm{sgs}}$, which require modelling. The filtered chemical source term, $\bar{S}_\alpha$, is also unknown. The tilde and overbar operators represent (density weighted) Favre filtering and standard spatial filtering, respectively. The LES equations are complemented by the equation of state for

an ideal gas

$$\bar{p} = \bar{\rho}\tilde{T}R_m \sum_{\alpha=1}^{N} \frac{\tilde{Y}_\alpha}{W_\alpha}, \tag{4}$$

where R_m is the universal gas constant, W_α the molecular weight of species α and N the number of species considered. The Smagorinsky model [14] is used to close the momentum equation in (1) as

$$\tau_{ij}^{\text{sgs}} + \frac{2}{3}\bar{\rho}k^{\text{sgs}}\delta_{ij} = -2\bar{\rho}\nu_t\left(\tilde{S}_{ij} - \frac{1}{3}\tilde{S}_{kk}\delta_{ij}\right), \tag{5}$$

where δ_{ij} is the Kronecker delta symbol, $\tilde{S}_{ij}$ is the resolved strain rate tensor and turbulent kinetic energy, k^{sgs}, is the solution to the quadratic equation

$$ak^2 + bk + c = 0, \tag{6}$$

using the coefficients $a = \frac{C_e}{\Delta}$, $b = \frac{2}{3}\tilde{S}_{kk}$ and

$$c = 2C_k\Delta\left(\tilde{S}_{ij} - \frac{1}{3}\tilde{S}_{kk}\right) : \tilde{S}_{ij}. \tag{7}$$

Model coefficients, C_e and C_k, are set to 1.048 and 0.094, respectively, and Δ is the filter width. Finally, the turbulent viscosity is computed as

$$\nu_t = C_k\Delta\sqrt{k^{\text{sgs}}} \tag{8}$$

which is utilised in (5) and also in the energy equation in (1) as $D_{\text{eff}} = \bar{\rho}(\nu + \nu_t)$.

3. Combustion modelling

The filtered reaction rate in (1), $\bar{S}_\alpha$, requires closure, which is at the heart of turbulent combustion modelling. This is done here using the aforementioned reaction-rate closure. Reactor models like Partially Stirred Reactor (PaSR) [4] and Eddy Breakup (EBU) model [15] use an eddy-diffusivity assumption to model TCI at the sub-grid level. Porumbel and Menon [8] note that reactor models have known limitations as:

(1) LES does not resolve sub-grid molecular fluxes, subgrid mixing and the effect on reaction kinetics
(2) Subgrid scalar fields, unlike turbulence, can be strongly anisotropic
(3) Reaction rate can be overestimated in regions of high shear.

These are shortcomings are addressed using the Linear Eddy Model (LEM) of Kerstein [16] which simulates (as opposed to models) fine scale diffusion and reaction kinetics on highly resolved one-dimensional (1D) domains. The LEM equations for temperature

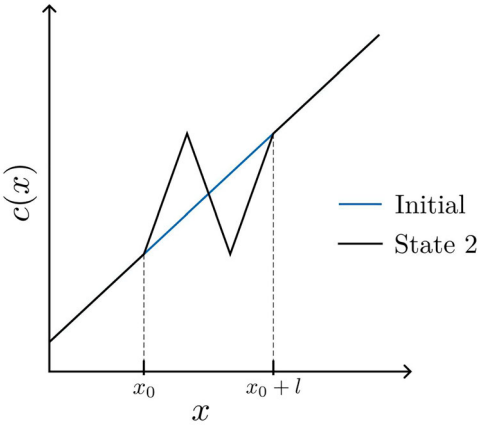

Figure 1. Concentration c profile along the LEM coordinate x, turbulent stirring is simulated by a single 'triplet map' rearrangement (state 2) starting at x_0 and spanning l units.

and species mass fractions are given by

$$\rho c_p \frac{\partial T}{\partial t} = -\frac{\partial Q}{\partial x} + S_T, \tag{9}$$

and

$$\rho \frac{\partial Y_\alpha}{\partial t} = -\frac{\partial j_{\alpha,x}}{\partial x} + S_\alpha, \tag{10}$$

with x being the 1D LEM coordinate, and Q and j_α the diffusion fluxes for temperature and species mass fraction, respectively. Species diffusivities are computed here assuming unity Lewis number, i.e. $Le = 1$ for all species without considering differential diffusion. However, since LEM equations are solved in physical space, utilising mixture averaged diffusion coefficients for individual components is straightforward. An important feature of LEM is that it simulates the effect of turbulent stirring through rearrangement events known as 'triplet maps'[2], shown here in Figure 1. These discrete events are implemented as a Poisson process in time and are controlled via eddy parameters location x_0, size l and frequency λ.

Eddy sizes and locations are also stochastic in nature with x_0 being sampled from a uniform distribution along the 1D line and l from the frequency distribution given by

$$f(l) = \frac{5}{3} \frac{l^{-8/3}}{\eta^{-5/3} - \Delta^{-5/3}}, \tag{11}$$

where η is the Kolmogorov dissipative scale that can be approximated as

$$\eta = N_\eta \frac{\Delta}{Re_\Delta^{3/4}}. \tag{12}$$

Here, $Re_\Delta = u'\Delta/\nu$ is the sub-grid Reynolds number and $u' = \sqrt{2k^{\text{sgs}}/3}$, which also determines the frequency of stirring events as

$$\lambda = \frac{54}{5} \frac{\nu Re_\Delta}{C_\lambda \Delta^3} \frac{\left[(\Delta/\eta)^{5/3} - 1\right]}{\left[1 - (\eta/\Delta)^{4/3}\right]}, \tag{13}$$

with λ having units [$m^{-1}s^{-1}$]. The model constants N_η and C_λ in Equations (12) and (13) control the scaling (between Δ and η) and the frequency of triplet maps as they relate to Re_Δ.

LEM, used as combustion closure in the LES context (known as LES-LEM), involves incorporating an LEM domain within each LES cell, which is time-advanced independently of the LES equations, typically within one LES time step. Combustion closure is achieved either by directly replacing $\tilde{Y}_\alpha$ from Equation (1) with the Favre-averaged Y_α from Equation (10), as described in previous studies [8,17,18], or by replacing the filtered chemical source terms in Equation (1) with its (Favre-averaged) LEM counterpart [19].

LES-LEM has been applied in the simulation of premixed combustion [8,19], non-premixed combustion [18], and scalar mixing [20], with minimal alteration to its formulation. Consequently, it is often considered to be a mode- and regime-independent combustion closure model. In the premixed context, LES-LEM offers several advantages over standard closure models: (1) utilisation of reaction kinetic data without filtering or artificial thickening; (2) simulation of turbulent burning rate rather than computation from a prescribed laminar flame speed, as in some flame speed models [e.g. 21]; and (3) the ability to transition LEM flame structures from laminar to corrugated flamelets and then to distributed reaction zones (with increasing k_{sgs}) without altering the formulation [22].

Although flame wrinkling is not explicitly modelled, LES-LEM allows for the existence of more than one flame front on an LEM domain at high enough k^{sgs}, where the radius of curvature can be approximated as half the distance between two flames [23]. However, the primary drawback of LES-LEM is the associated computational cost, as each LES cell now contains a highly resolved LEM domain, requiring reaction advancement for each discrete LEM 'wafer'. This challenge has prompted the development of a recently introduced variant called super-grid LEM (SG-LEM) [2], which is discussed below in some detail.

3.1. *Super-grid LEM (SG-LEM)*

SG-LEM is a computation speed-up technique for LES-LEM where the LES mesh is coarse-grained to form a super-grid (SG) consisting of LES cell clusters. Instead of advancing an LEM domain in each LES cell, they (LEM domains) are embedded in each cluster and are now responsible for reaction-diffusion and also turbulent stirring via triplet maps. The new method employs a variant of the LES-LEM splicing algorithm [20] using SG-resolved fluxes and also accounts for varying cluster sizes in the domain. Figure 2 is a schematic of the SG-LEM concept, including LEM-state changes driven by a splicing operation.

The salient features of the SG-LEM splicing scheme are as follows: (1) LEM domains have designated 'in-splice' (attachment) and 'out-splice' (detachment) ends; (2) the length of an LEM fragment 'out-spliced' from an LEM domain that corresponds to one of the faces of its associated cluster is proportional to the total outgoing flux computed at that face; (3) detachments from an LEM domain are ordered in ascending order of flux at the associated faces; (4) similarly, attachment operations are ordered in descending order of associated fluxes. This flux-ordered splicing was directed by the principle of control volume crossing-rate, where a higher flux must result in a greater displacement of the LEM fragments within the SG. The reader is directed to reference [2] for details regarding the implementation of SG splicing. Finally, the individual LEM subdomain provides chemical state data *in-situ*, which is used for a mapping-type closure, described below.

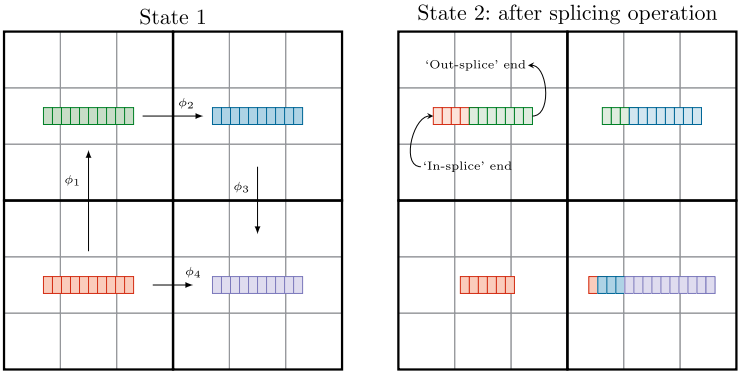

Figure 2. SG-LEM schematic showing initial and final states after a splicing operation. Thin grey boxes represent LES cells; thick black boxes represent SG clusters; coloured boxes show LEM domains comprised of LEM wafers; the arrows marked ϕ_1-ϕ_4 show fluxes resolved by the flow solver, where arrow lengths represent flux magnitude.

3.1.1. *Mapping closure with SG-LEM*

The SG-LEM mapping closure is similar to the RIF (Representative Interactive Flamelets) [24] model in that it uses chemical state data (derived from LEM advancement) that are conditionally binned on primitive variables. More precisely, LEM domains generate unique solution tables for each cluster, with the primitive variables acting as state-space, which can then be used to compute the filtered chemical state at LES resolution. This is achieved by weighted moments of probability density functions (PDFs) for the said primitives, computed individually for each cell in a cluster. For premixed combustion, 'progress variable' c serves as the lone primitive, defined in this study as

$$c = \frac{Y_{\mathrm{O}_2} - Y^u_{\mathrm{O}_2}}{Y^b_{\mathrm{O}_2} - Y^u_{\mathrm{O}_2}}, \tag{14}$$

where superscripts u and b denote unburnt and burnt values, respectively. A transport equation for the Favre mean value $\tilde{c}$ is advanced as

$$\frac{\partial \bar{\rho}\tilde{c}}{\partial t} + \frac{\partial \bar{\rho}\tilde{u}_j\tilde{c}}{\partial x_j} = \frac{\partial}{\partial x_j}\left(-\left[\nu + \frac{\nu_t}{Sc_t}\right]\frac{\partial \bar{\rho}\tilde{c}}{\partial x_j}\right) + \overline{\dot{\rho}\dot{c}}, \tag{15}$$

with a filtered source term $\overline{\dot{\rho}\dot{c}}$, and Sc_t is the turbulent Schmidt number, set to 0.7 for this study. LES-filtered mass fractions are then computed using the weighted first moment of a Favre PDF for c as

$$\tilde{Y}_\alpha(\mathbf{x}, t) = \int_0^1 \langle Y_\alpha \mid c\rangle \, \tilde{P}(c)\, \mathrm{d}c, \tag{16}$$

using the local (LEM-generated) mass fractions that are conditionally averaged in c, written here as $\langle Y_\alpha \mid c\rangle$ for species α. The Favre PDF $\tilde{P}$ defined as

$$\tilde{P} = \frac{\int_0^1 \rho(c) P(c) \mathrm{d}c}{\int_0^1 \rho(c)\, \mathrm{d}c}$$

and is presumed as a β function, i.e. $\tilde{P}(c) = \beta(\tilde{c}, \widetilde{c''^2})$, which requires a model for the variance $\widetilde{c''^2}$ in addition to the transport Equation (15) for the mean value of c. Here, the

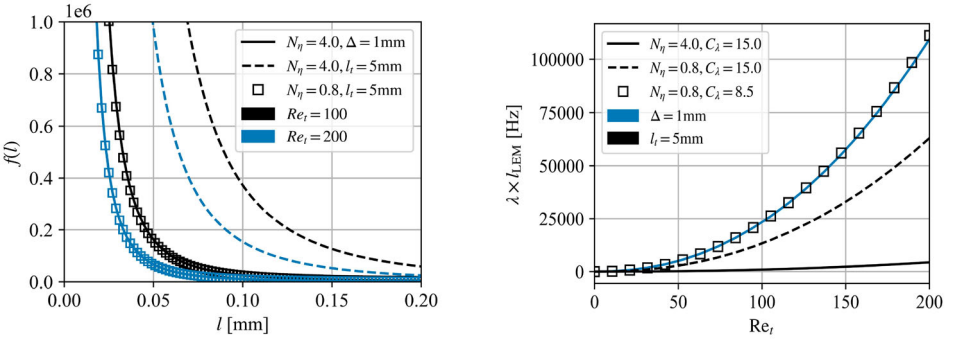

Figure 3. Eddy size distribution (a) and stirring frequency (b) controlled by LEM constants. Assumed viscosity of 1×10^{-5}Pa s.

algebraic model by Pierce and Moin [25] is used. The source term for mean progress variable is obtained similarly using the first moment as

$$\bar{\dot{c}}(\mathbf{x}, t) = \int_0^1 \langle \dot{c} \mid c \rangle \, \tilde{P}(c) \, \mathrm{d}c. \tag{17}$$

Conditional mass fractions as a function of reaction progress, i.e. the aforementioned solution tables, are initialised with a steady-state laminar (premixed) flamelet solution using an in-house code. LEM domains then continually update these tables during run-time, allowing each cluster to obtain flame structure data that is informed by local turbulence conditions, as well as combustion driven flow physics via splicing. The LEM equations (11), (12) and (13) are also modified to use the cluster size $l_{t,\mathrm{LEM}} = \sqrt[3]{V_\mathrm{c}}$ instead of Δ as the largest eddy size, V_c being the volume of the cluster.

A secondary output allows for diagnosing LEM states using the Favre-mean reported at SG resolution, i.e.

$$\tilde{\psi}_{\mathrm{LEM}} = \frac{\sum_\gamma \rho_\gamma \psi_\gamma}{\sum_\gamma \rho_\gamma}, \tag{18}$$

where γ is the LEM wafer index, and ψ is any thermochemical scalar such as T or Y_α.

The LEM model defines and depends on model constants N_η and C_λ (cf. Section 3). We now introduce a means of adjusting the literature values for the LEM constants to SG-LEM, since, unlike LES-LEM, the assumed largest length scale which can be represented on a SG cluster is larger than the filter width, as determined by mesh agglomeration. Suppose this length scale in the SG-LEM context is larger than the LES-LEM filter width by a factor of 5, N_η must be scaled by 0.2 to maintain the Kolmogorov scale estimate, as given by Equation (12). This also retains the size distribution given by (11), which can be seen in Figure 3(a) as it compares $N_\eta = 4$ and 0.8 using length scales of $\Delta = 1$ mm and $l_t = 5$ mm. Then, C_λ is adjusted to retain the eddy frequency given as a function of the turbulent Reynolds number, shown in Figure 3(b).

LEM operator-splitting used in this work is termed 'blocked-sequencing' in Ref. [2]. Here, stochastic Poisson processes determine the number of triplet map events to be implemented for an LES time-step Δt, and they are then implemented *sequentially*

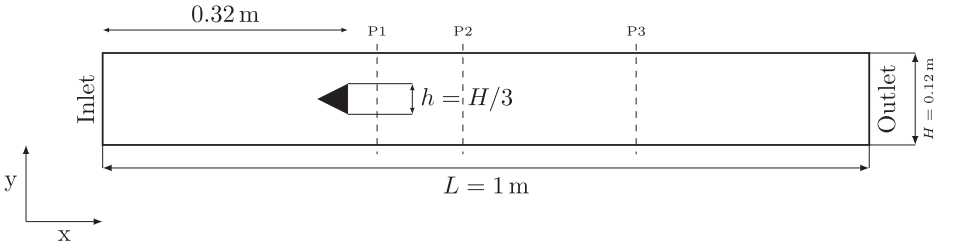

Figure 4. The Volvo validation rig setup, spanwise width is 0.24 m. Not shown are the pre-inlet section and round exhaust pipe. Dashed lines show measurement planes P1, P2 and P3 at $x = 0.95$ h, 3.75 h and 9.4 h measured from the base of the bluff-body.

without pause. This is followed by reaction-diffusion advancement in a classical Strang-splitting method for the time step as $\mathbf{D}^{\Delta t/2}\mathbf{R}^{\Delta t}\mathbf{D}^{\Delta t/2}$. Symbols **D** and **R** refer to diffusion and reaction advancement, respectively. The alternative is to perform reaction-diffusion advancement between successive rearrangements as they are sampled and implemented in time; this results in frequent start-restart cycles for stiff numerical integration subroutines, which can be a significant computational overhead at high k^{sgs} values[3]. Further details of LEM advancement (operator splitting), chemistry advancement, coarse-graining and binning procedures are reported in Ref. [2] and are not repeated here for brevity.

4. Test case and numerical setup

The presented case is known as the 'Volvo validation rig' in the literature. The setup involves turbulent, premixed, propane-air combustion in a straight-walled channel, with flame stabilisation behind a triangular bluff body (flame-holder). A schematic representation of the case is shown in Figure 4. The pre-inlet section (not shown) consists of air supply, fuel supply, fuel distribution by means of a critical orifice plate, and a honeycomb screen to induce turbulence. The setup vents out to a round pipe (0.45 m diameter, also not shown). Optical windows allow diagnostic access, and the available data consists of gas analysis [5], velocity measurements using laser Doppler Velocimetry (LDV) [6], and coherent anti-Stokes Raman scattering (CARS) [7] spectroscopic measurements. The set of parameters studied experimentally, known as Case 1, are summarised in Table 1.

4.1. *Numerical setup*

A pressure based solver was implemented using the `OpenFOAM` library [26] (v. 9) using second order numerical schemes for temporal and for spatial discretization. Pressure-velocity coupling is achieved using the PISO (Pressure-implicit with splitting of operators) methodology of Issa et al. [27] using two inner-correctors. Resulting linear systems of equations from the implicit discretization of the transport equations are solved using the preconditioned (bi)-conjugate gradient (PCG/PBiCG) solvers from `OpenFOAM`, for symmetric/asymmetric matrices. The computational domain resembles Figure 4 with steady inflow conditions applied at the inlet and a non-reflecting (wave-transmissive) pressure outlet. Periodic boundary conditions are applied to the spanwise coordinate. The computational mesh is composed exclusively of hexahedral cells having a uniform side length of 1 mm in the flame region, larger cells are used upstream of the bluff-body (side 4 mm) and grading is used to resolve some of the boundary layer on all sides of the bluff body

Table 1. Volvo validation rig, Case 1.

Parameter		Value
Inflow pressure	p_0 [atm]	1.0
Inflow temperature	T_0 [K]	288
Inflow velocity	v_0 [ms^{-1}]	17.6
Reynolds number	$Re = v_0 h/\nu$	46.59×10^3
Equivalence ratio	ϕ	0.62
Laminar flame speed	s_u [ms^{-1}]	0.15
Integral length scale	l_t [m]	4×10^{-3}
Velocity fluctuations	v_{RMS} [ms^{-1}]	7.8
Karlovitz Number	Ka	62.0
Damkölher Number	Da	0.7
Temperature ratio	T_b/T_u	5.90

(min size 0.4 mm). Cell sizes are similar to those used in Ref. [11], where it is deemed adequate to capture the required flow features and turbulent scales. Furthermore, it facilitates a direct comparison with PaSR results reported in [11]. The OpenFoam utility 'blockMesh' was used to generate the multi-block mesh consisting around 9.9 million grid cells.

As for LEM-advancement, an implicit second-order finite-difference scheme is used for diffusion advancement while the stiff numerical integrator `CVODE` [28] is used for chemistry advancement. SG mesh agglomeration was achieved using the well established `MGRIDGEN` [29] library functions. Clustering parameters include the minimum and maximum number of cells to agglomerate. The β-PDF shapes are interpolated at runtime from a pre-tabulated PDF table of $200 \times 200 \times 200$ values corresponding to $\tilde{c}$, $\widetilde{c''^2}$ and c.

4.2. *Super-grid parameters*

The objective of this study is twofold: firstly, to test the performance SG-LEM for a high Reynolds number setup and, secondly, to understand its response to coarse-graining parameters, thereby identifying limitations of the present framework. The target capability of the fully developed model is to combine large cluster sizes, highly resolved LEM domains, with detailed chemistry in order to fully leverage the speed-up offered by coarse-graining. However, the framework could also be used for highly resolved LES studies where chemical state results are of less importance and instead focus on reactive flow structures, in which case the framework should be tested for small cluster sizes and with global mechanisms; hence, the following types of simulations were attempted:

(1) A 'fine' cluster resolution of 64 using a two-step global mechanism with 5 species from Ghani et al. [30].
(2) The fine cluster using using a skeletal mechanism (Z66) from Zettervall et al. [11] with 12 species and 66 irreversible reactions.
(3) A 'medium' cluster resolution of 125 using Z66.
(4) A 'coarse' cluster resolution of 250 using Z66.
(5) A 'coarser' cluster resolution of 1000, also using Z66.

Both Refs. [11,30] report LES studies of the Volvo case, albeit for different purposes. While [30] use a highly refined mesh ($\approx$ 20M cells) to study acoustic perturbations, [11]

Table 2. Simulation parameters.

Sim.	SGcluster size	kinetics	Flame stabilisation	Core-hours
1	64	2-step		7500
2	125	Z66	ICS + Cluster shape control	60,000
3	250	Z66	ICS + Cluster shape control	30,000
3*	250	Z66	Cluster shape control	30,000

studies the effect of reaction mechanisms on temperature and concentration fields, as well as validates the presented Z66 kinetics.

While the fine cluster (using global chemistry) produced a stable flame, the use of Z66 with any cluster size did not produce a stable flame. Investigation of this behaviour led to the conclusion that the more accurate (in terms of chemistry) Z66 mechanism was more sensitive to inaccuracies in splicing transport that are strongly influenced by SG parameters. In particular, excessive (splicing) entrainment of cold free stream fluid behind the recirculation zone lead to excessive cooling of the reactive mixture on LEM domains in the region which is reflected in the LES resolved mapping results. In order to mitigate these effects, the following two methods were employed to stabilise the flame.

4.2.1. *Flame stabilisation*

(1) *Intra-cluster stirring (ICS):* While splicing models large-scale advection and triplet maps represent small-scale advection, advective structures of cluster size dimensions are not included in the SG-LEM formulation in [2]. In this work, an *ad-hoc* method for simulating these advective structures is achieved by implementing, on all LEM domains, one additional eddy per time step assuming $\eta = l_{t,\mathrm{LEM}}/2$ before usual LEM advancement.

(2) *Cluster shape control:* While there is no direct way instruct `MGRIDGEN` to agglomerate LES cells to form regular and repeatable cluster shapes, an indirect method is realised through domain decomposition. As `MGRIDGEN` independently performs the agglomeration of SG clusters on each processor domain, the shape of the processor domain can be used to constrain the agglomeration to, e.g. produce flow-aligned clusters. The shapes of the clusters significantly impact splicing, which is the sole means by which LEM domains 'feel' large-scale transport. A 'structured' decomposition method is used to achieve this where the outlet face is first decomposed using the 'scotch' [31] method followed by projection in the streamwise direction. The `OpenFOAM` utility `decomposePar` was used to accomplish this. The entire domain is decomposed using the scotch method when cluster shape control is not utilised.

The above methods were tested independently and then together. As a result, all but the coarsest cluster size (1000) showed stable flames. Table 2 lists the simulations used for further analysis. Note that, despite stabilisation, the use of Z66 with cluster size 64 was too slow to simulate the required number of flow passes given available compute resources; hence, it was not considered for analysis.

For all cases, automatic time-stepping was used to maintain a Courant number of 0.6. LEM domains were resolved at a 'DNS-like' 50 μm to capture TCI and the LEM constants $N_\eta = 0.8$ and $C_\lambda = 8.7$ were used – based on modifications discussed in Section 3.

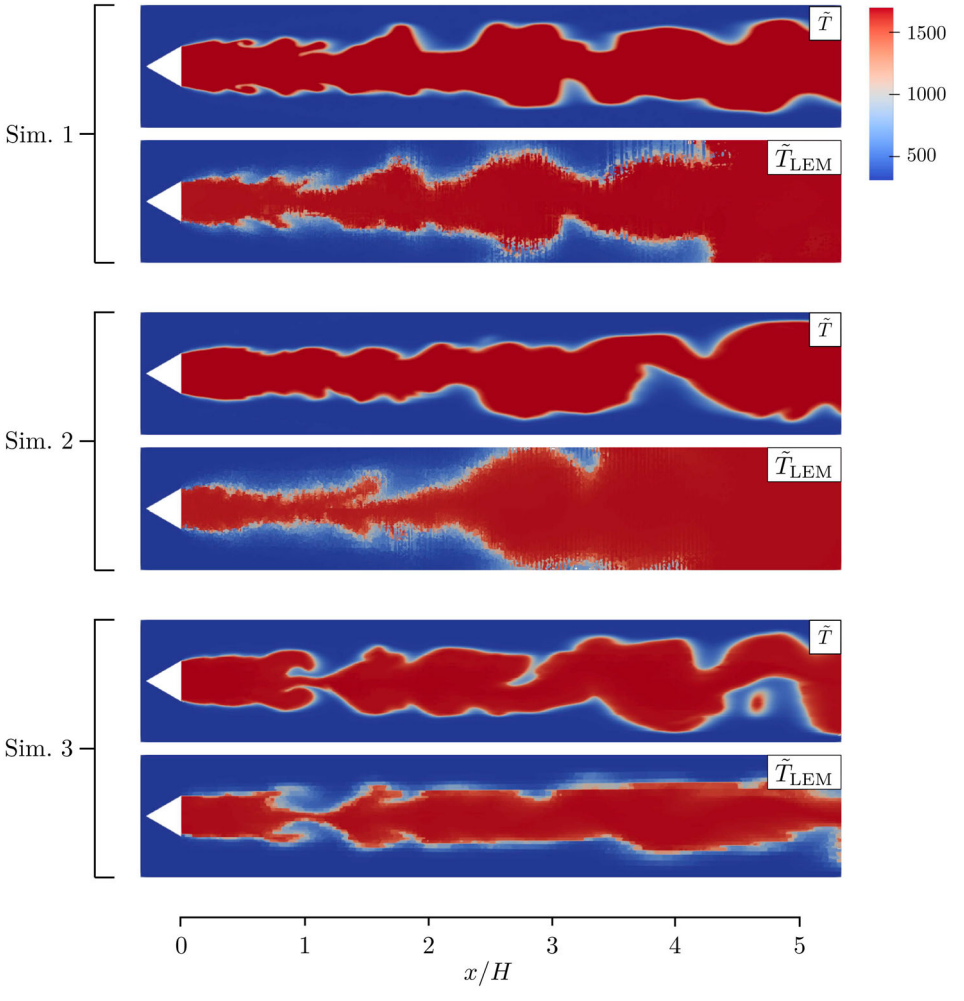

Figure 5. Instantaneous temperature for plane $z = 0$. LES resolved $\tilde{T}$ iterated from enthalpy $\tilde{H}$ and Equation (16). LEM state temperature $\tilde{T}_{\mathrm{LEM}}$ reported at SG resolution using Equation (18).

Furthermore, species mass fractions are binned into 200 equally-spaced c-bins for mapping closure. Simulations were run for 1.5 s ($\approx$ 25 flow through times) and data for time averaging was collected for 0.5 s.

5. Results and analysis

SG-LEM in essence is a multi-scale closure for LES. The following sections analyse mapping closure results and LEM domain states. This is followed by a comparison with experimental data.

5.1. *Flow structures and LEM states*

Mapping closure using SG-LEM ultimately depends on the accurate evolution of the mean progress variable. Reaction progress at the LES and SG levels relies on fluxes resolved

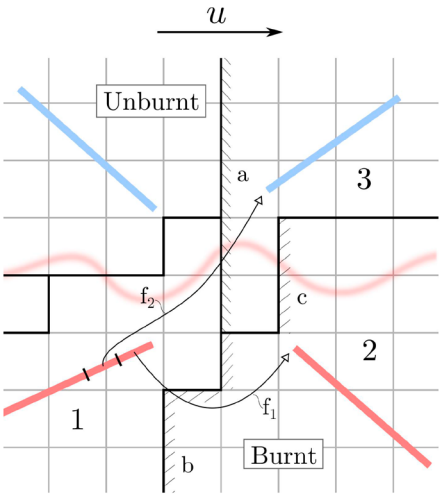

Figure 6. Large scale transport between LEM domains for agglomerated meshes.

on the two levels, as they determine the splicing transport of the fuel-air mixture as well as combustion products. Figure 5 compares instantaneous temperature at the two resolutions for simulations 1, 2, and 3. The LES temperature field ($\tilde{T}$) results from advancing the enthalpy equation in (1) and the filtered concentration fields from Equation (16) utilising the caloric equation of state. Concurrently, LEM domain temperatures ($\tilde{T}_{\mathrm{LEM}}$), given by Equation (18), are reported as the secondary output at SG resolution. LES fields are smooth whereas LEM states are noisy as they reflect the combined effect of chemistry advancement, triplet maps and splicing. Figure A1 (Appendix) shows the ratio of resolved and total total turbulent kinetic energy for this mesh, and Figure A2 (Appendix) shows the number of triplet map implemented in the domain.

LES temperature fields are qualitatively identical for all three simulations, however, differences in the LEM states can be observed owing to the SG setup. Sim. 1, using small clusters, shows very similar structures in the primary and secondary outputs. This occurs until around $x/H = 4.2$ where the secondary output shows an increased spread for LEM domains in the y coordinate. The spreading artifact is more pronounced for Sim. 2 where LEM states diverge from the LES solution slightly before $x/H = 3$. This spread is not observed for Sim. 3 and the SG high temperature region, i.e. LEM states, remains roughly parallel to the walls. This clearly shows the effect of cluster shape control on splicing, in this case Sim. 3 provides the best adjacency of the LEM and LES flame fronts. The increased flame spread and the previously observed extinction behaviour (when ICS and shape control were not used for Z66) originate from inaccuracies in splicing transport. This has been identified as a limitation in the current SG-LEM framework. The previous application in Ref. [2] did not exhibit such a sensitivity to SG cluster size and shapes. Splicing inaccuracies and their relation to cluster shapes are explained as follows.

5.1.1. *Super-grid splicing performance*

Consider the situation in Figure 6: a resolved flame front, shown by the red curve, divides the burnt and unburnt regions, with a flux u acting from left to right. Automated clustering

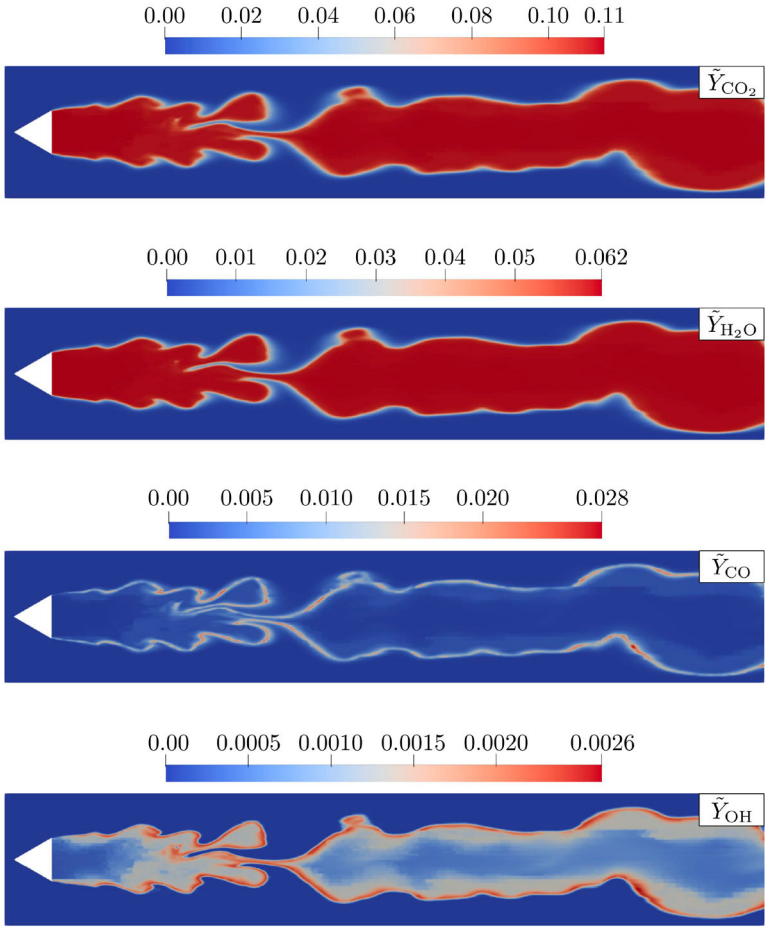

Figure 7. Instantaneous mapping closure for Sim. 3.

results in non-standard shapes, unlike those implied by Figure 2. Examining the splicing transport between domains '1', '2' and '3', we observe fragment 'f1' being spliced between domains 1 and 2 via SG face 'b'. Similarly, fragment 'f2' is spliced from domain 1 to 3 via face 'a'. If domains 1 and 2 contain burnt products, fragment 'f2' represents a spurious transport instance of burnt products into domain 3. In LES resolved splicing, as in standard LES-LEM, fragment 'f2' would remain in the burnt region. Here, since attachment and detachment occur at designated ends, fragment 'f2' will remain in LEM domain 3 for a longer time, creating additional flame fronts, before being spliced into domain 2 via face 'c'. A similar explanation can be given for the entrainment of bulk fluid into the recirculation zone. Essentially, the shape and size of SG clusters influence residence times for spliced fragments using the current splicing scheme. Excessive entrainment led to flame quenching issues, this is counteracted by additional length scale breakdowns imposed by the ICS subroutine, which helps stabilise the flame for Sim. 2. Although such splicing artifacts could be reduced by careful and solution-dependent clustering, practical applications with complex geometries favour unstructured grids which requires the automated clustering algorithms such as `MGRIDGEN`. Cluster shape control, as presented in Sim. 3, requires

a priori knowledge of the flame orientation and flow behaviour. Further improvements of results, which are left for future investigations, are expected to be achievable with more sophisticated splicing schemes. One such could be the incorporation of a 'cross term' that relates to sub-grid (w.r.t. the super-grid) velocities, similar to the procedure described in Section 10.6.2 of Ref. [32].

5.2. *Mapping closure*

Mapping closure results for Sim. 3 are shown in Figure 7 where major species CO_2 and H_2O are smoothly varying physical fields, similar to Figure 5. However, intermediate species CO and OH show slight blocky artifacts that reveal the underlying SG structure. These are similar to those reported in Ref. [2] and are attributed to variations in c-conditioned values for such intermediate species across cluster boundaries. These variations reflect LEM advancement influenced by splicing and triplet maps. Unlike major species, the apparent noise is not entirely smoothed out by the β-PDF due to their slow chemical timescales.

5.3. *Scalar profiles*

Figures 8, 9 and 11 compare mean and RMS LES results with experimental data, as well as data from a reference PaSR simulation from [11] that uses a similar mesh with 12 million grid points, the Z66 skeletal mechanism and a transport equation for k^{sgs} and dynamically computed C_k and C_e. All scalars are averaged over the spanwise z coordinate. Temperature and velocities are normalised.

Mean axial velocity along the centreline ($y=0, z=0$) is shown in Figure 8. SG-LEM simulations capture the downstream velocities better than PaSR but with a weaker recirculation in the near field behind the wedge, where the PaSR model shows very good agreement. Figure 9 shows mean scalar profiles for planes P1, P2 and P3. Weaker recirculation produced by SG-LEM can also be seen at P1 here for all three simulations. As this is common to both reaction mechanisms, it can be inferred that the behaviour stems from a combination of mesh parameters and mapping closure for the progress variable source

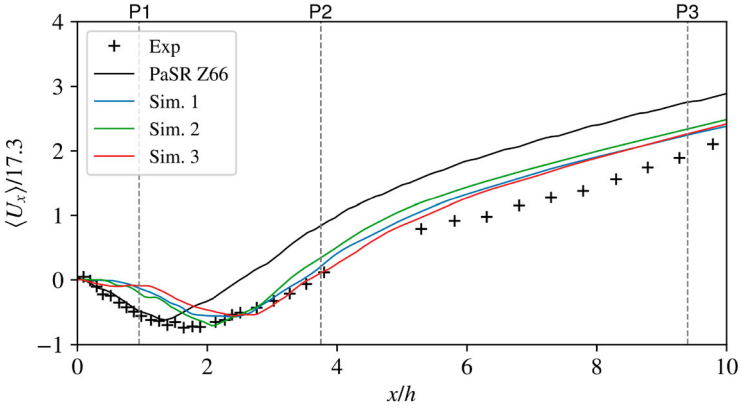

Figure 8. Centreline mean u_x velocity, cf. Figure 4 for plane positions and Table 2 for simulation setup.

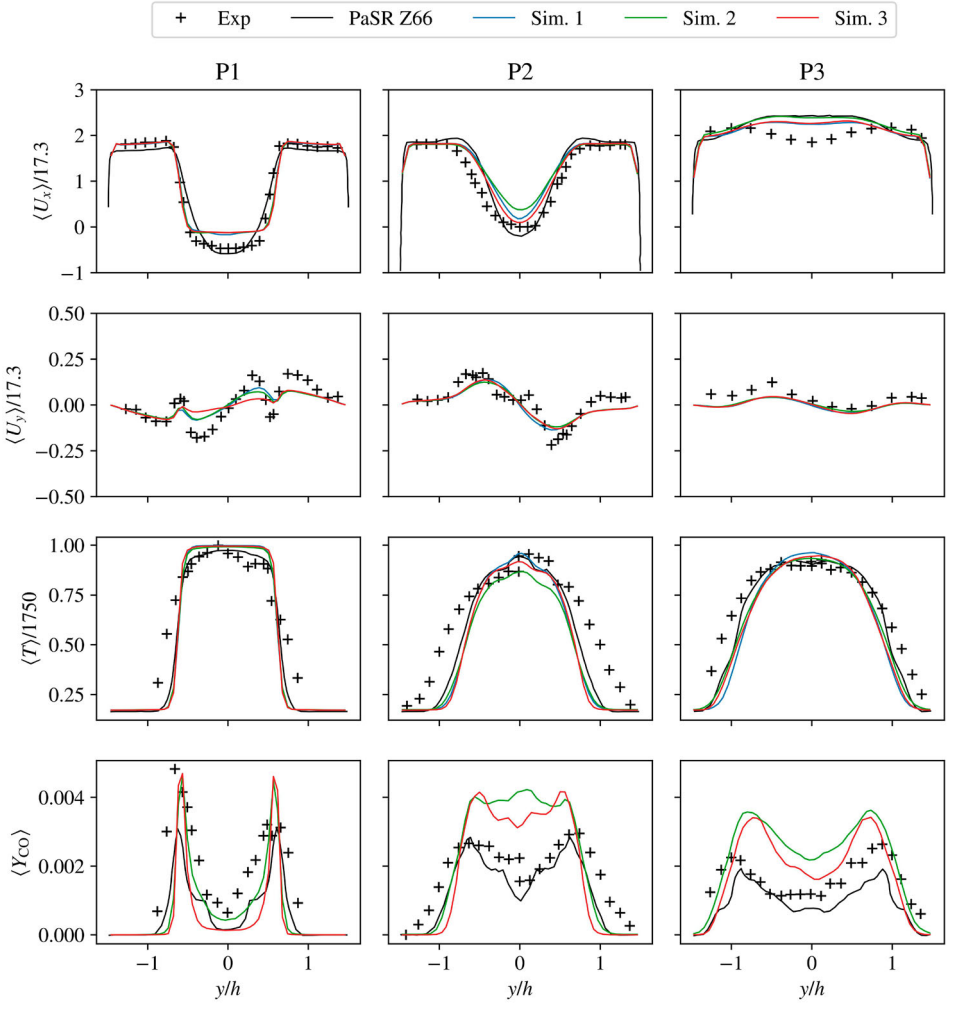

Figure 9. Mean scalar profiles, experimental data from Ref. [5], and PaSR data from Ref. [11].

term. Far-field velocity profiles at P3 show similar results for PaSR and SG-LEM, centreline velocities driven by dilatation are overestimated by both methods. Velocity in the transverse plane (second row) exhibits the correct trends, PaSR data was not available for comparison here.

Temperature profiles (third row) are in good agreement with experiment overall. Both methods capture the transition from plateau-shaped to U-shaped profiles between P1 and P2. However, SG-LEM exhibits a slightly flatter profile at P1. The elevated temperature here drives thermal expansion which explains the higher axial velocities at P1, also seen in Figure 8. Slight differences can be observed between Sim. 2 and Sim. 3 at P2, alluding to the differences in the SG structure. Mean CO profiles (fourth row) using the Z66 mechanism[4] show clear differences between PaSR and SG-LEM, where the latter shows better agreement with experiment at P1 but elevated levels of CO behind the recirculation zone at P2 and P3.

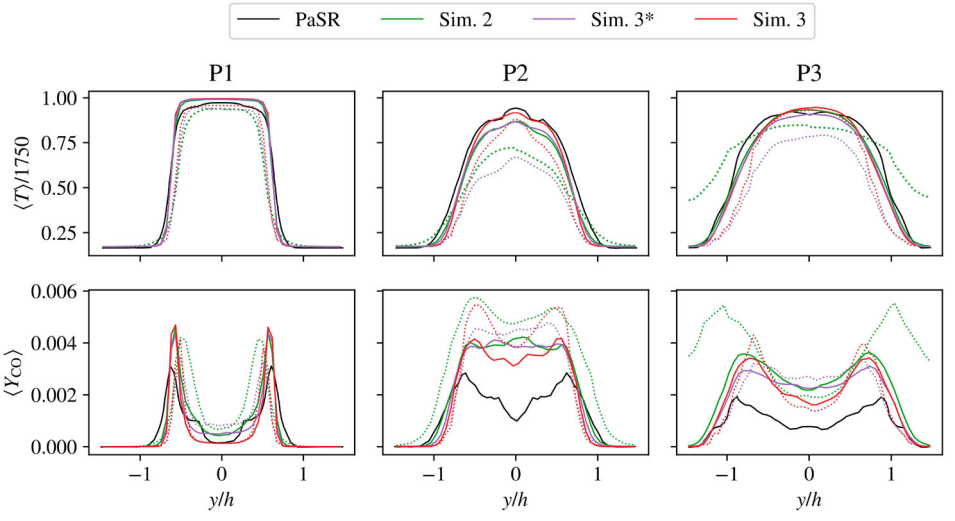

Figure 10. Comparison of mean LES results and LEM states. Dotted lines are obtained from Equation (18), reported at SG resolution and time-averaged.

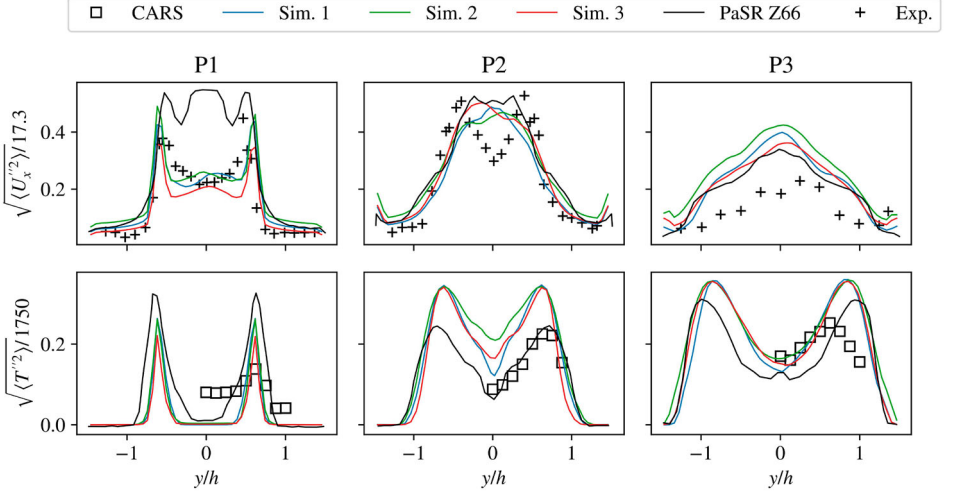

Figure 11. RMS velocity and temperature at planes P1, P2 and P3 (cf. Figure 4). CARS data from Sjunnesson et al. [7].

To better understand these results and the relations among the presumed PDF mapping closure, LEM advancement and splicing, LES scalar profiles are compared to time-averaged LEM states given by Equation (18) shown in Figure 10. Dotted lines indicate mean (time-averaged) LEM states at SG resolution. The effect of SG cluster shapes is apparent in this secondary output. Profiles for temperature and CO look similar at P1 for all simulations. At P2, however, lower LEM temperatures can be observed for Sim. 2 as well as elevated LEM CO levels. This indicates higher entrainment of free stream fluid via splicing for Sim. 2, and hence the need for ICS which, although it promotes flame stability, still results in a slower conversion of CO. The spreading artifact described in

Section 5.1.1 is also apparent for Sim. 2 at P3, in both temperature and CO. Note, however, that LES-resolved temperature is still in agreement with PaSR and experiment as they are determined by LES-resolved $\tilde{c}$, which implies mean $\tilde{c}$ profiles are correct. Thus, the elevated CO values in the LES solution for Sims. 2 and 3 must originate from the LEM states influenced by splicing transport and excessive entrainment. Finally, the influence of ICS can be seen in comparing Sim. 3 and 3* – even though it was not required to stabilise the flame (Sim. 3*), lower LEM temperatures and higher CO levels at P2 and P3 result from fewer length-scale breakdowns of the LEM scalar field. Overall, Sim. 3 using both the shape control and ICS shows the best agreement with PaSR and experiments.

RMS profiles for axial velocity and temperature in Figure 11. SG-LEM shows good agreement for the RMS velocity at P1. Further downstream, the performance is similar to that of PaSR, profiles indicate predicted transient fluctuations in the burnt gases by all simulations as being higher than observed in experiment. RMS temperature levels (bottom row) are over-predicted overall, with SG-LEM being slightly more accurate in the near field. PaSR is notably more accurate at P2. The higher temperature fluctuations shown by Sim. 2 at P2 could be the result of increased bulk flow entrainment at this SG resolution. These, however, are challenging diagnostics for reacting simulations, and inaccuracies in experimental data can also factor in. Given this, the model is deemed to perform well overall.

5.4. *Computational performance*

While runtime information on the PaSR simulation in [11] is not available, the computational demand of SG-LEM relative to a reactor model is straightforward to estimate as it scales with the ratio of the number of LES cells to LEM wafers in the domain, especially given the blocked-sequence eddy implementation used in this work. Using Sim. 3 as an example, LEM domains across all clusters contain $\approx$ 4.4 million wafers, while the LES grid consists of 9.9 million cells; hence, the chemistry advancement demand for Sim. 3 is roughly half of that of a reactor model. Other sources of compute demand are associated with advancing transport equations for each species in a reactor model, and also of PDF shape generation (interpolated vs. computed on-the-fly) for SG-LEM.

6. Conclusion and future work

SG-LEM achieves computational speed-up of traditional LES-LEM techniques using coarse-graining of the LES mesh, on-the-fly chemistry tabulation, and a presumed PDF approach that requires a transport equation for mean progress variable, as well as a suitable scalar variance model. In this work, we present a follow-up to Menon et al. [2] with further validation of the SG-LEM method using the Volvo validation rig, consisting of rectangular walls and a triangular flame-holder. Super-grid structure and its influence on model performance was investigated which led to a clearer understanding of the model limitations and highlighted areas of improvement. Compared to the previous application, there is less chemical-state validation data, however, the case is of high Reynolds number and exhibits features of combustion in real-world devices. Case 1 of the Volvo rig was simulated using super-grid (SG) cluster sizes of 64, 125 and 250. Modifications to the LEM constants are suggested since, unlike traditional LES-LEM, the assumed integral length scale could be several fold the LES filter width. The larger geometry and lower temperature of the fuel-air mixture of the Volvo case revealed limitations of the SG splicing algorithm, used to

simulate large-scale transport on LEM domains, that were not revealed by the initial validation in Ref. [2]. In particular, excessive entrainment of cold free stream fluid behind the recirculation zone leads to unphysical quenching of the flame when simulated with an accurate Z66 skeletal mechanism. A simple global mechanism was also tested with cluster size 64 that did not produce such quenching behaviour.

Two methods were developed in this work to mitigate SG splicing inaccuracies and improve flame stability: (1) an *ad-hoc* stirring enhancement to simulate advective structures that are neither resolved by splicing nor by LEM triplet maps termed Intra-cluster stirring (ICS); and (2) an indirect method to produce flow-aligned SG cluster shapes using domain decomposition which reduces numerical diffusion by SG splicing. Time-averaged and RMS fluctuations for temperature, axial velocity and CO mass fractions were compared to experiment was well as a reference PaSR solution using Z66. While both ICS and shape control produced stable flames, the effect of cluster shapes was evident in mean LEM profiles for temperature and CO at downstream locations– standard SG generation resulted in greater flame spread (on LEM domains) in the flame-normal direction. However, LES resolved temperature and velocity profiles were in good agreement with experiments for all SG-LEM simulations as they are determined by the mean progress variable field. Elevated CO levels were observed for SG-LEM using Z66, even with flow-aligned cluster shapes. Comparison with LEM CO levels led to the conclusion that, even though splicing accuracy was improved, some excessive entrainment (splicing) of free-stream fluid was enough to delay conversion of CO in the axial direction.

In the previous application, a premixed ethylene-air DNS case [2], SG-LEM demonstrated superior results for minor species CO and OH compared to PaSR. Such capability could not be demonstrated here due to SG splicing inaccuracies compounded by the larger geometry. Splicing, especially for large cluster sizes, has been identified as the main limitation for the current framework and, therefore, future research on SG-LEM must focus on this issue. As computational speed-up scales with cluster size, it is more attractive to use large cluster sizes for cases with detailed chemistry. The stabilisation techniques developed in this work illuminate potential pathways for further improving the framework. Future versions of SG-LEM could use an overset super-grid designed using physical criteria instead of mesh agglomeration. Alternatively, a more sophisticated splicing scheme can be conceptualised where attachment and detachment points are varied along the LEM domain to better relate the residence times of spliced fragments with fluid residence times within clusters, in contrast to fixed points used in the current scheme. A more well defined intra-cluster stirring scheme is also required where large triplet maps are sampled according to the LES resolved vortical structures. Such measures would contribute to a robust SG-LEM framework which can fully utilise the benefits of a powerful technique like LEM a cost-effective manner.

Notes

1. Summation is assumed for Roman letters such as indices i and j, but not Greek letters such as α
2. Note that the term ‘map’ has two distinct meanings in this work: (1) ‘triplet map’ for rearrangement events in the LEM domain, and (2) ‘mapping-closure’ for LES resolved fields, which is described in a later section.
3. While the blocked routine introduces a splitting error, stand-alone LEM simulations performed for the tested propane-air mixture showed negligible differences between blocked and Strang-splitting for conditionally binned data, when small time steps were employed.

4. The global mechanism used in Sim. 1 was validated for laminar flame speed and adiabatic temperature in [30], and not for chemical closure.

Disclosure statement

No potential conflict of interest was reported by the author(s).

Funding

The authors would like to acknowledge the compute and storage resources provided by the Chalmers Centre for Computational Science and Engineering (C3SE), part of the Swedish National Infrastructure for Computing (SNIC), which was used in the this study. It was partially funded by the Swedish Research Council through grant agreement no. 2018-05973.

References

[1] C. Fureby, *Large eddy simulation of combustion instabilities in a jet engine afterburner model*, Combust. Sci. Technol. 161(1) (December 2000), pp. 213–243. ISSN 0010–2202

[2] A.M. Menon, M. Oevermann, and A.R. Kerstein, *A super-grid approach for LES combustion closure using the linear eddy model*, Combust. Theory Model. 28(1) (January 2024), pp. 99–126. ISSN 1364–7830.

[3] A.R. Kerstein, *A linear-eddy model of turbulent scalar transport and mixing*, Combust. Sci. Technol.60(4-6) (August 1988), pp. 391–421. ISSN 0010-2202, 1563-521X.

[4] J. Chomiak, *Combustion a Study in Theory, Fact and Application*, Abacus Press, Philadelphia, USA, January 1990.

[5] A. Sjunnesson, S. Olovsson, and B. Sjöblom, *Validation Rig- a tool for flame studies*, in *10th International Symposium on Air Breathing Engines*, Nottingham, England, 1991, pp. 385–393.

[6] A. Sjunnesson, C. Nelsson, and E. Max, *LDA measurements of velocities and turbulence in a bluff body stabilized flame*, Tech. Rep., December 1991

[7] A. Sjunnesson, P. Henrikson, and C. Löfström, *CARS measurements and visualization of reacting flows in a bluff body stabilized flame*, in *28th Joint Propulsion Conference and Exhibit*, American Institute of Aeronautics and Astronautics, Nashville, TN, United States

[8] I. Porumbel and S. Menon, *Large eddy simulation of bluff body stabilized premixed flame*, in *44th AIAA Aerospace Sciences Meeting and Exhibit*, American Institute of Aeronautics and Astronautics, Reno, Nevada, January 2006. ISBN 978-1-62410-039-0

[9] C. Fureby and C. Löfström, *Large-eddy simulations of bluff body stabilized flames*, Symp. Combust. Proc. 25(1) (1994), pp. 1257–1264. ISSN 00820784

[10] C. Fureby, *A comparative study of large eddy simulation (LES) combustion models applied to the Volvo validation rig*, in *55th AIAA Aerospace Sciences Meeting*, American Institute of Aeronautics and Astronautics, Grapevine, Texas, January 2017. ISBN 978-1-62410-447-3

[11] N. Zettervall, K. Nordin-Bates, E.J.K. Nilsson, and C. Fureby, *Large eddy simulation of a premixed bluff body stabilized flame using global and skeletal reaction mechanisms*, Combust. Flame 179 (May 2017), pp. 1–22. ISSN 0010–2180.

[12] S. Arshad, *Large eddy simulation of combustion using linear-eddy subgrid modeling*, PhD thesis, Chalmers University of Technology, Göteborg, Sweden, 2019

[13] E. Gonzalez, A. Dasgupta, S. Arshad, and M. Oevermann, *Effect of the turbulence modeling in large-eddy simulations of nonpremixed flames undergoing extinction and reignition*, in *55th AIAA Aerospace Sciences Meeting*, American Institute of Aeronautics and Astronautics, Grapevine, Texas, January 2017. ISBN 978-1-62410-447-3

[14] J. Smagorinsky, *General circulation experiments with the primitive equations: I. The basic experiment*, Mon. Weather Rev. 91(3) (March 1963), pp. 99–164. ISSN 1520-0493, 0027–0644.

[15] D.B. Spalding, *Mixing and chemical reaction in steady confined turbulent flames*, Symp. Combust. Proc. 13(1) (January 1971), pp. 649–657. ISSN 0082–0784.

[16] A.R. Kerstein, *Linear-eddy modeling of turbulent transport. Part 4. Structure of diffusion flames*, Combust. Sci. Technol. 81(1-3) (January 1992), pp. 75–96. ISSN 0010-2202, 1563-521X.

[17] T.M. Smith and S. Menon, *Subgrid combustion modeling for premixed turbulent reacting flows*, in *36th AIAA Aerospace Sciences Meeting and Exhibit*, American Institute of Aeronautics and Astronautics, Reno, NV, U.S.A., January 1998
[18] W.H. Calhoon and S. Menon, *Subgrid modeling for reacting large eddy simulations*, in *34th Aerospace Sciences Meeting and Exhibit*, American Institute of Aeronautics and Astronautics, Reno, NV, U.S.A., January 1996
[19] S. Arshad, E. Gonzalez-Juez, A. Dasgupta, S. Menon, and M. Oevermann, *Subgrid reaction-diffusion closure for large eddy simulations using the linear-eddy model*, Flow Turbul. Combust. 103(2) (August 2019), pp. 389–416. ISSN 1573–1987.
[20] S. Arshad, B. Kong, A.R. Kerstein, and M. Oevermann, *A strategy for large-scale scalar advection in large eddy simulations that use the linear eddy sub-grid mixing model*, Int. J. Numer. Methods Heat Fluid Flow 28(10) (October 2018), pp. 2463–2479. ISSN 0961–5539.
[21] P. Flohr and H. Pitsch, *A turbulent fame speed closure model for LES of industrial burner fows*, in *Proceedings of the Summer Program*, Center for Turbulence Research, Stanford, CA, United States, 2000, pp. 169–179
[22] T.M. Smith and S. Menon, *One-dimensional simulations of freely propagating turbulent premixed flames*, Combust. Sci. Technol. 128(1-6) (October 1997), pp. 99–130. ISSN 0010–2202.
[23] S. Menon and A.R. Kerstein, *Stochastic simulation of the structure and propagation rate of turbulent premixed flames*, Symp. Combust. Proc. 24(1) (January 1992), pp. 443–450. ISSN 0082–0784.
[24] C. Hasse, H. Barths, and N. Peters, *Modelling the effect of split injections in diesel engines using representative interactive flamelets*, SAE Technical Paper 1999-01-3547, SAE International, Warrendale, PA, October 1999
[25] C.D. Pierce and P. Moin, *A dynamic model for subgrid-scale variance and dissipation rate of a conserved scalar*, Phys. Fluids 10(12) (December 1998), pp. 3041–3044. ISSN 1070-6631, 1089–7666.
[26] H.G. Weller, G. Tabor, H. Jasak, and C. Fureby, *A tensorial approach to computational continuum mechanics using object-oriented techniques*, Comput. Phys. 12(6) (November 1998), pp. 620–631. ISSN 0894–1866.
[27] R.I. Issa, A.D. Gosman, and A.P. Watkins, *The computation of compressible and incompressible recirculating flows by a non-iterative implicit scheme*, J. Comput. Phys. 62(1) (January 1986), pp. 66–82. ISSN 0021–9991.
[28] A.C. Hindmarsh, P.N. Brown, K.E. Grant, S.L. Lee, R. Serban, D.E. Shumaker, and C.S. Woodward, *SUNDIALS: suite of nonlinear and differential/algebraic equation solvers*, ACM Trans. Math. Softw.31(3) (September 2005), pp. 363–396. ISSN 0098–3500.
[29] I. Moulitsas and G. Karypis, *Serial/Parallel library for generating coarse grids for multigrid methods*, Tech. Rep., December 2001
[30] A. Ghani, T. Poinsot, L. Gicquel, and G. Staffelbach, *LES of longitudinal and transverse self-excited combustion instabilities in a bluff-body stabilized turbulent premixed flame*, Combust. Flame 162(11) (November 2015), pp. 4075–4083. ISSN 00102180.
[31] F. Pellegrini and J. Roman, *Scotch: A software package for static mapping by dual recursive bipartitioning of process and architecture graphs*, in *High-Performance Computing and Networking*, H. Liddell, A. Colbrook, B. Hertzberger, and P. Sloot, eds., Springer, Berlin, Heidelberg, 1996, pp. 493–498. ISBN 978-3-540-49955-8.
[32] S. Menon and A.R. Kerstein, *The linear-eddy model*, in *Turbulent Combustion Modelling: Advances, New Trends and Perspectives*, Springer, Netherlands, 2011. pp. 221–247.

Appendix

Figure A1 shows the ratio of resolved to total turbulent kinetic energy. The resolved component is computed as

$$k^{\text{res}} = \frac{1}{2} u_i' u_i', \tag{A1}$$

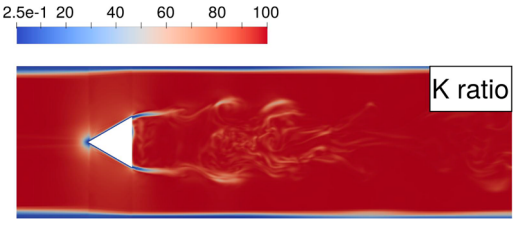

Figure A1. Ratio of resolved to total turbulent kinetic energy for Sim. 3

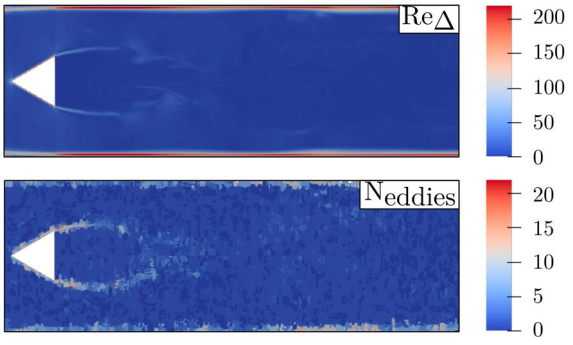

Figure A2. Number of triplet maps (bottom) implemented in an LES time step with local turbulent Reynolds number (top) for Sim. 2.

where u_i' is RMS velocity and subgrid k^{sgs} is obtained from the Smagorinsky momentum closure. The ratio of resolved to the total turbulent kinetic energy is reported as a percentage in Figure A1, i.e. $\frac{k^{\text{res}}}{k^{\text{res}}+k^{\text{sgs}}} \times 100$

Figure A2 shows eddy events (triplet maps) that were implemented during an LES time step ($\approx 4 \times 10^{-6}$ s) where the frequency and size distribution are informed by Re_Δ. The LEM constants in Table 2 were used because literature values from [2] showed no implemented eddies for the case.